Article:

Oncomodulin regulates spontaneous calcium signalling and maturation of afferent innervation in cochlear outer hair cells

Yang Yang[1] (iD), Kaitlin Murtha[1], Leslie K. Climer[1] (iD), Federico Ceriani[2] (iD), Pierce Thompson[1], Aubrey J. Hornak[1], Walter Marcotti[2,3] (iD) and Dwayne D. Simmons[1,2,4] (iD)

[1] *Department of Biology, Baylor University, Waco, TX, USA*
[2] *School of Biosciences, University of Sheffield, Sheffield, UK*
[3] *Sheffield Neuroscience Institute, University of Sheffield, Sheffield, UK*
[4] *Department of Integrative Biology and Physiology, University of California, Los Angeles, CA, USA*

The Journal of Physiology

Abstract Cochlear outer hair cells (OHCs) are responsible for the exquisite frequency selectivity and sensitivity of mammalian hearing. During development, the maturation of OHC afferent connectivity is refined by coordinated spontaneous Ca^{2+} activity in both sensory and non-sensory cells. Calcium signalling in neonatal OHCs can be modulated by oncomodulin (OCM, β-parvalbumin), an EF-hand calcium-binding protein. Here, we investigated whether OCM
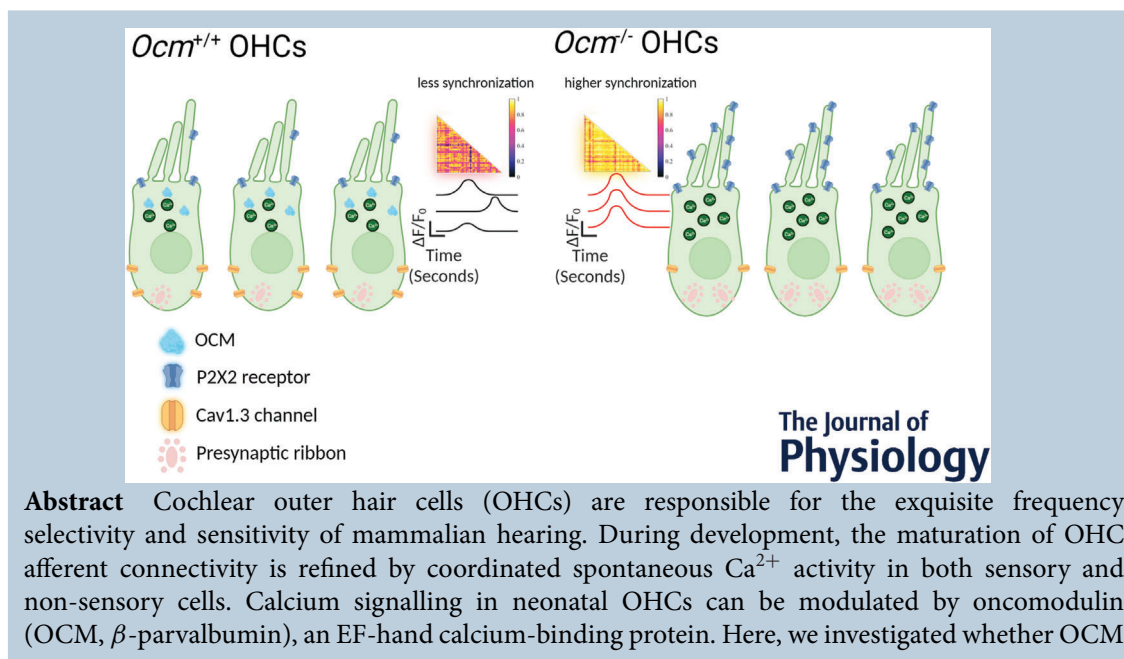
Yang Yang received his PhD in Biology at Baylor University. https://sites.baylor.edu/simmonslab His research mainly focuses on investigating calcium signalling in mammalian hair cells and understanding the role of calcium-binding proteins in both hair cell development and normal hearing maintenance.

regulates OHC spontaneous Ca^{2+} activity and afferent connectivity during development. Using a genetically encoded Ca^{2+} sensor (GCaMP6s) expressed in OHCs in wild-type ($Ocm^{+/+}$) and Ocm knockout ($Ocm^{-/-}$) littermates, we found increased spontaneous Ca^{2+} activity and upregulation of purinergic receptors in OHCs from $Ocm^{-/-}$ cochlea immediately following birth. The afferent synaptic maturation of OHCs was delayed in the absence of OCM, leading to an increased number of ribbon synapses and afferent fibres on $Ocm^{-/-}$ OHCs before hearing onset. We propose that OCM regulates the spontaneous Ca^{2+} signalling in the developing cochlea and the maturation of OHC afferent innervation.

Correspondence author D. D. Simmons: Department of Biology, Baylor University, 101 Bagby Ave, Waco, TX, USA. Email: dwayne_simmons@baylor.edu

Abstract figure legend Oncomodulin (OCM) modulates Ca^{2+} activity in immature outer hair cells (OHCs). The lack of OCM increases spontaneous Ca^{2+} activity and changes the expression of $Ca_v1.3$ channels and purinergic receptors in OHCs during development. The maturation of afferent synapses in OHCs is delayed due to the absence of OCM, resulting in an upregulation of ribbon synapses in $Ocm^{-/-}$ OHCs before hearing onset. We propose that OCM is crucial for modulating Ca^{2+} activity in developing OHCs.

Key points

- Cochlear outer hair cells (OHCs) exhibit spontaneous Ca^{2+} activity during a narrow period of neonatal development. OHC afferent maturation and connectivity requires spontaneous Ca^{2+} activity.
- Oncomodulin (OCM, β-parvalbumin), an EF-hand calcium-binding protein, modulates Ca^{2+} signals in immature OHCs.
- Using transgenic mice that endogenously expressed a Ca^{2+} sensor, GCaMP6s, we found increased spontaneous Ca^{2+} activity and upregulated purinergic receptors in $Ocm^{-/-}$ OHCs.
- The maturation of afferent synapses in $Ocm^{-/-}$ OHCs was also delayed, leading to an upregulation of ribbon synapses and afferent fibres in $Ocm^{-/-}$ OHCs before hearing onset.
- We propose that OCM plays an important role in modulating Ca^{2+} activity, expression of Ca^{2+} channels and afferent innervation in developing OHCs.

Introduction

The regulation and control of Ca^{2+} is a major challenge for cochlear sensory cells during development as well as in the adult. Similar to other sensory systems, the developing cochlea exhibits intrinsically generated, sound-independent spontaneous Ca^{2+} activity that is critical for the maturation and refinement of neural circuits (Babola et al., 2021; Blankenship & Feller, 2010; Clause et al., 2014; Lippe, 1994). The mammalian cochlea has two types of specialized sensory cells, which are involved in the transduction of sound into electrical responses (Dallos, 1992). Inner hair cells (IHCs) relay sound information via glutaminergic synapses onto type I afferent spiral ganglion neurons. Outer hair cells (OHCs) enhance cochlear sensitivity and frequency tuning of the cochlear partition and are primarily innervated by cholinergic medial olivocochlear neurons that form a sound-evoked acoustic reflex (Guinan, 2018).

Additionally, OHCs form synapses onto type II afferent spiral ganglion neurons that may be activated by traumatic noise exposures (Flores et al., 2015; Liu et al., 2015). In rodents, the maturation of OHC innervation patterns occurs during the first and second postnatal weeks (Simmons, 1994; Simmons et al., 1996). Recent studies show that the OHC innervation is refined by coordinated spontaneous Ca^{2+} activity. Ca^{2+} waves initiated in the greater epithelial ridge (GER), or Kölliker's organ, a developmentally transient structure located adjacent to the row of IHCs, synchronize the spontaneous Ca^{2+} activity in OHCs through the modulation of voltage-gated Ca^{2+} channels and purinergic receptor signalling (Ceriani et al., 2019; Jeng et al., 2020). However, little is known about the intracellular Ca^{2+} signalling network that modulates OHC spontaneous Ca^{2+} activity during cochlear maturation.

A multitude of transporters, pumps, exchangers and calcium-binding proteins (CaBPs) are integral to the Ca^{2+}

signalling network in OHCs and tightly regulate Ca^{2+} activity and homeostasis. Oncomodulin (OCM), a small EF-hand CaBP of approximately 12 kDa, is the β isoform of parvalbumin and shares at least 53% sequence identity with α-parvalbumin (Banville & Boie, 1989). Previous studies show that in the cochlea, OCM is expressed specifically by OHCs and preferentially localizes to the lateral membrane, the basal portion of the hair bundle and the basal pole adjacent to efferent terminals (Simmons et al., 2010). After hearing onset, which in most altricial rodents occurs at around postnatal day 12 (P12), OHCs express high levels of OCM (2–3 mM) compared to other CaBPs (Hackney et al., 2005). Together, this suggests that OCM may have a specific function that differs from other CaBPs in OHCs. OCM is an important CaBP for which targeted deletion causes hearing loss (Pangrsic et al., 2015; Tong et al., 2016). The absence of OCM alters Ca^{2+} signalling in OHCs before the onset of hearing (Murtha et al., 2022), revealing a major role of OCM in regulating Ca^{2+} activity during maturation. Given that spontaneous Ca^{2+} activity plays a critical role in OHC development, we hypothesized that OCM modulates spontaneous Ca^{2+} activity during development.

To investigate how OCM regulates spontaneous Ca^{2+} activity in developing OHCs, we expressed a genetically encoded, tissue-specific Ca^{2+} sensor (*Atoh1*-GCaMP6s) in *Ocm* wild-type ($Ocm^{+/+}$) and *Ocm* knockout ($Ocm^{-/-}$) mice. $Ocm^{-/-}$ mice exhibited early onset hearing loss, and their OHCs showed faster KCl-induced Ca^{2+} transients than those recorded from $Ocm^{+/+}$ mice and other mouse strains (Climer et al., 2021; Murtha et al., 2022; Tong et al., 2016). In neonatal mice (P2), we observed spontaneous Ca^{2+} activity in OHCs that was synchronized by Ca^{2+} waves elicited in the GER. However, $Ocm^{-/-}$ OHCs exhibited higher synchronization and stronger fractional change of GCaMP6s fluorescence intensity ($\Delta F/F_0$) during Ca^{2+} activity in the GER, compared to $Ocm^{+/+}$ OHCs. We also found that the expression of P2X2, one of the main purinergic receptors in the cochlea, was upregulated in $Ocm^{-/-}$ cochlea. $Ocm^{-/-}$ OHCs showed delayed synaptic pruning with an increased number of tunnel crossing fibres during development. We propose that the lack of OCM alters the spontaneous Ca^{2+} activity via ATP signalling and affects the afferent maturation and innervation of the OHCs.

Methods

Ethical approval

Animals were bred at the Baylor University Vivarium. The animal work was licensed by the Institutional Animal Care and Use Committee (IACUC), Baylor University as established by U.S. Public Health Service.

Animals

All mouse colonies were purchased from The Jackson Laboratory (Bar Harbor, ME, USA). For these studies, *Atoh1*-GCaMP6s mouse lines were maintained on mixed backgrounds. We first crossed *Ocm* wildtype ($Ocm^{+/+}$) and *Ocm* knockout ($Ocm^{-/-}$) mice with B6;129S-*Gt(ROSA)26Sor^{tm96.1(CAG-GCaMP6s)Hze}*/J, Ai96 (RCL-GCaMP6s) or Ai96, which contains a floxed-STOP cassette preventing transcription of the GCaMP6 slow variant Ca^{2+} indicator. These mice were then crossed with knock-in transgenic mice expressing Cre recombined from the *Atoh1* locus (Chen et al., 2013). *Atoh1*-driven Cre GCaMP6s mice showed tissue-specific expression of endogenous green fluorescence (Cox et al., 2012; Mulvaney & Dabdoub, 2012; Yang et al., 2010). We utilized GCaMP6s positive $Ocm^{+/+}$ and $Ocm^{-/-}$ mice to monitor intracellular Ca^{2+} activities directly after acute dissection.

Cochlear function assays

For measurement of distortion product otoacoustic emissions (DPOAEs), adult mice were anaesthetized with xylazine (20 mg/kg, I.P.) and ketamine (100 mg/kg, I.P.). Acoustic stimuli were delivered using a custom acoustic assembly previously described (Maison et al., 2012). Briefly, two electrostatic earphones (EC-1, Tucker Davis Technologies, Alachua, FL, USA) were used to generate primary tones and a Knowles miniature microphone (EK-3103, Knowles Electronics, Itasca, IL, USA) was used to record ear-canal sound pressure. Stimuli were generated digitally with 4 s sampling. Ear-canal sound pressure and electrode voltage were amplified and digitally sampled at 20 s for analysis of response amplitudes. Both outputs and inputs were processed with a digital I-O board (National Instruments (Austin, TX, USA) PXI-4461). For measurement of DPOAEs at $2f_1 - f_2$, the primary tones were set so that the frequency ratio (f_2/f_1) was 1.2 and so that f_2 level was 10 dB below f_1 level. For each f_2/f_1 primary pair, levels were swept in 10 dB steps from 20 dB SPL to 80 dB SPL (for f_2). At each level, both waveform and spectral averaging were used to increase the signal-to-noise ratio of the recorded ear-canal sound pressure, and the amplitude of the DPOAE at $2f_1 - f_2$ was extracted from the averaged spectra, along with the noise floor at nearby points in the spectrum. Iso-response curves were interpolated from plots of DPOAE amplitude *vs.* sound level. The threshold was defined as the f_2 level required to produce a DPOAE at 0 dB SPL. Right ears were used for all hearing tests.

Tissue preparation

Cochleae were harvested from $Ocm^{+/+}$ or $Ocm^{-/-}$ mice of either sex at postnatal day (P)2, P6, P10 and 3–4 weeks

as previously described (Murtha et al., 2022). Briefly, pups were euthanized by rapid induction of hypothermia, and apical coil OHCs were dissected from the organ of Corti in an extracellular medium composed of (in mM): 136.8 NaCl, 5.4 KCl, 0.4 KH_2PO_4, 0.3 Na_2HPO_4, 0.8 $MgSO_4$, 1.3 $CaCl_2$, 4.2 $NaHCO_3$, 5 HEPES and 5.6 glucose. The pH was adjusted to 7.4–7.5 (osmolality ∼306 mmol/kg). The apical coil was then transferred to a small microscope chamber with nylon mesh fixed to a stainless-steel ring on the bottom and visualized using an upright microscope (DM 6000 FS, Leica Microsystems, Wetzlar, Germany) with a ×63 water immersion objective (Leica).

Confocal Ca^{2+} imaging

Ca^{2+} signals from GCaMP6s were recorded at room temperature with 480 nm excitation wavelength (X-Light V2 spinning disk confocal, 89 North Inc, Williston, VT, USA. PRIME95B Photometrics Cooled sCMOS with 95% QE, Teledyne Photometric, Tucson, AZ, USA). Images were taken using VisiView (Visitron, Puchheim, Germany) and analysed offline using ImageJ (NIH). Ca^{2+} signals were measured as relative changes in fluorescence emission intensity ($\Delta F/F_0$) and calculated by MATLAB (The MathWorks, Natick, MA, USA). $\Delta F = F - F_0$, where F is fluorescence at time t and F_0 is the fluorescence at the onset of the recording.

For spontaneous Ca^{2+} activity, GCaMP6s positive cochlea was recorded immediately after acute dissection. Each GCaMP6s fluorescence recording consisted of 1103 frames taken at 6 frames/s from a 912×912 pixels region. For the region of interest (ROI), a circle centred on each OHC (diameter 5 μm) was drawn. For the ROI in the GER, the ROI was drawn outlining the maximum area of each multicellular Ca^{2+} event. The maximum spread of the Ca^{2+} event in the GER (longitudinal extension length) from calibrated images was then measured with ImageJ. Fluorescence traces were computed as pixel averages from each ROI and $\Delta F/F_0$ was calculated in MATLAB. The mean GCaMP6s fluorescence of the first 50 frames was used as baseline (F_0). A Savitzky–Golay filter was then applied to smooth the $\Delta F/F_0$ and increase the signal-to-noise ratio of Ca^{2+} signals (window length = 11, polynomial order = 1). A spike inference algorithm in MATLAB was used to estimate the spike count and position. Only the peak above 4 standard deviations of baseline was calculated ($F_0 + 4 \times$ SD, shown as a dashed line in Figs 4 and 5). The minimum peak distance was 5 frames. The mean frequency was then computed by dividing the number of spikes by the total duration of the recording. We calculated the pairwise Spearman's rank correlation coefficient (r_S) between every pair of OHCs in the field of view during the spontaneous Ca^{2+} waves in the GER (time window 2), or during the absence of Ca^{2+} activity in the GER (time window 1). The mean of Spearman's rank correlation coefficient (r_{avg}) was calculated from r_S after Fisher's z-transformation:

$$z = \text{arctanh}\,(r_S)$$

$$r_{avg} = \tanh\,(z_{avg})$$

z_{avg} is the mean of the transformed z values. r_{avg} was then used for the liner regression with corresponding spread along the cochlear spiral; and F-test was used to determine if the slope is significantly non-zero.

KCl depolarization solution contained (in mM): 142.4 KCl, 0.4 KH_2PO_4, 0.3 Na_2HPO_4, 0.8 $MgSO_4$, 1.3 $CaCl_2$, 4.2 $NaHCO_3$, 5 HEPES and 5.6 glucose. The pH was adjusted to 7.4–7.5 (osmolality ∼305 mmol/kg). ATP depolarization solution was diluted from 100 mM stock ATP (Thermo Fisher Scientific, Waltham, MA, USA) with the extracellular solution (800 μM ATP for working solution). Pyridoxalphosphate-6-azophenyl-2′,4′-disulfonic acid (PPADS; Sigma-Aldrich, St Louis, MO, USA) and nifedipine (Sigma-Aldrich) were dissolved with dimethyl sulfoxide and then diluted using the extracellular solution. Ca^{2+}-free medium composed of (in mM): 136.8 NaCl, 5.4 KCl, 0.4 KH_2PO_4, 0.3 Na_2HPO_4, 0.8 $MgSO_4$, 4.2 $NaHCO_3$, 5 HEPES, 5.6 glucose and 1 EGTA, pH adjusted to 7.4–7.5 (osmolality ∼306 mmol/kg). Depolarization solution was delivered to the chamber using a PMD-D35 perfusion/media exchange system (Tokai Hit, Shizuoka, Japan).

For Ca^{2+} transients, the perfusion system started 8 s after the imaging started; 100 μl of KCl depolarization solution, or 100 μl of ATP was added into a microscope chamber containing 300 μl extracellular solution (1:4 dilution, ∼40 μM K^+ final concentration, or 200 μM ATP final concentration in the chamber), followed by a 2 min perfusion with the extracellular solution to help with equilibration. Image data were collected 8 s before drug delivery and for 3 min after drug delivery. To avoid the disturbance from spontaneous Ca^{2+} activity, only the fluorescence signals from OHCs that reach maximum intensity between 8 and 60 s were calculated. For the nifedipine or PPADS experiments, the blocker was added to the explant right before ATP or KCl application. Each GCaMP6s fluorescence recording includes 1500 frames taken at 80 frames/s from a 1200×1200 pixels region. After background subtraction, the activated OHCs were computed as pixel means using ImageJ. The calcium transient time constant (τ) was determined.

Genotyping and qRT-PCR

DNA was extracted from mouse tail samples using Extract-N-Amp™ Tissue PCR Kit (Sigma-Aldrich). PCR primers used for genotyping are listed below:

Atoh1-Cre primer pair forward: 5′-CCGGCAGAGT TTACAGAAGC-3′, reverse: 5′-ATG TTT AGC TGG CCC AAA TG-3′; Cre control primer pair forward: 5′-CTA GGC CAC AGA ATT GAA AGA TCT-3′; reverse: 5′-GTA GGT GGA AAT TCT AGC ATC ATC C-3′; GCaMP6s primer pair forward: 5′-ACG AGT CGG ATC TCC CTT TG-3′; reverse: 5′-AGA CTG CCT TGG GAA AAG CG-3′; *Ocm* primer pair forward: 5′-CTC CAC ACT TCA CCA AGC AG-3′, reverse: 5′-TTT CAT GTT CAG GGA TCA AGT G-3′; *Ocm* deletion primer pair forward: 5′-CTC CAC ACT TCA CCA AGC AG-3′, reverse: 5′-GCT TGG GGA CCC CCT GTC TTC A-3′.

Cochleae from both ears were acutely dissected after anaesthesia and transferred to the lysis buffer. Total RNA was extracted using RNeasy plus Micro kits (Qiagen, Germantown, MD, USA). iScript$^{\text{TM}}$ Advanced cDNA Synthesis Kit (Bio-Rad Laboratories, Hercules, CA, USA) was used for reverse transcription.

qRT-PCR was performed using the SYBR Green PCR Master Mix Kit (Bio-Rad) as previously described (Murtha et al., 2022). Briefly, the *b2m* gene was used as a reference gene (Melgar-Rojas et al., 2015). Quantification of expression (fold change) from the C_q data was calculated following the $\Delta\Delta C_q$ method (Schmittgen & Livak, 2008), and normalized to the C_q value in $Ocm^{+/+}$ at P0. $2^{-\Delta\Delta C_q}$ was calculated to represent the relative expression (fold change).

Primers used for qRT-PCR are as follows: *b2m* forward 5′-TGGTCTTTCTGGTGCTTGTC-3′ and reverse 5′-GGG TGG AAC TGT GTT ACG TAG-3′; *Ocm* forward 5′-ATG AGC ATC ACG GAC ATT CTG AGC-3′ and reverse 5′-CTG GCA GAC ATC TTG GAG AGG C-3′; *CACNA1D* forward 5′-GCA AAC TAT GCA AGA GGC ACC AGA C-3′ and reverse 5′-CTT TGG GAG AGA GAT CCT ACA GGT G-3′; *P2RX2* forward 5′-GCG TTC TGG GAC TAC GAG AC-3′ and reverse 5′-ACG TAC CAC ACG AAG TAA AGC-3′ (PrimerBank ID 27544798a1). *P2RX3* forward 5′-CAA CAC AAC AAG TTT GAA CCC AGC-3′ and reverse 5′-AGG CTT CTT TAG CTT CTC ACTG-3′, *P2RX7* forward 5′-CCC TGC ACA GTG AAC GAG TA-3′ and reverse 5′-CGT GGA GAG ATA GGG ACA GC-3′.

Immunofluorescence microscopy

Histological analysis and immunocytochemistry were applied as previously described (Murtha et al., 2022). Briefly, cochleae from neonatal mice were flushed with 4% paraformaldehyde and then fixative overnight at 4°C, followed by three washes in phosphate-buffered saline, then blocked in 5% normal horse serum for 1 h at room temperature. Samples were stained with antibodies to OCM (Santa Cruz Biotechnology, Dallas, TX, USA, sc-7446, 1:200), P2X2 (Alomone Labs, Jerusalem,

Israel, APR-003, 1:400), the C-terminal-binding protein 2 (CtBP2, BD Biosciences, San Jose, CA, cat. no. 612044, 1:200) and peripherin (Sigma-Adrich, AB1530, 1:200). Primary antibodies were incubated overnight at 37°C. Appropriate Alexa Fluor (Thermo Fisher Scientific, 1:200) and Northern Lights (R&D Systems, Minneapolis, MN, USA, 1:200) conjugated secondary antibodies were incubated for 1 h at 37°C. Slides were prepared using Vectashield mounting medium with 4′,6-diamidino-2-phenylindole (DAPI; Vector Laboratories, Burlingame, CA, USA). Images were acquired using the LSM800 microscope using a high-resolution, oil-immersion objective (Zeiss). Cohorts of samples were immunostained at the same time and imaged under the same optical conditions to allow for direct comparison.

Western blotting

Dissected cochleae were harvested (3 cochleae in the same tube, total $n = 9$ for each genotype) and immediately placed into a lysis buffer containing: 1% Triton X-100, 25 mM Tris, pH 7.4, 150 mM NaCl, 1 mm dithiothreitol, 1 mm MgCl$_2$, 1 mM phenylmethylsulfonyl fluoride, and 1× protease inhibitor cocktail (Thermo Fisher Scientific). Samples were incubated on ice for 10 min and vigorously vortexed twice at 15 s interval. Lysates were spun down at 4°C 12,000 *g* for 20 min. Total protein concentration was determined using a BCA Protein Assay Kit (Thermo Fisher Scientific). The supernatant was diluted in sample buffer (Bio-Rad, 355 mM β-mercaptoethanol added) and heated for 30 min at 37°C. Samples (25 μg total protein) were subject to SDS-PAGE and protein was transferred to a polyvinylidene difluoride membrane. Membranes were blocked with 2.5% fish gelatin for 1 h at room temperature and incubated overnight at 4°C with primary antibody to rabbit P2X2R (1:400; Alomone Labs), mouse Ca$_v$1.3 (Thermo Fisher Scientific, 1:100), and rabbit β-tubulin (1:1000). After washing, membranes were incubated with appropriate horse-radish peroxidase-conjugated secondaries (anti-rabbit 1:7,500, anti-mouse 1:100) for 1 h at room temperature. Clarity Max ECL Substrate (Bio-Rad) was used to detect chemiluminescence via a ChemiDoc imaging system. Relative protein expression levels (normalized to β-tubulin) were determined by densitometric analysis using FIJI software.

Statistical analysis

Statistical analysis was performed using GraphPad Prism 9 (GraphPad Software, San Diego, CA, USA) and MATLAB software. Statistical comparisons of means were made by *t* test or, when normal distribution could not be assumed, the Mann–Whitney *U*-test. For multiple comparisons,

one-way or two-way ANOVA followed by Bonferroni post test was used unless otherwise stated. Data are given as means ± SD. Animals of either sex were randomly assigned to the different experimental groups. No statistical methods were used to define the sample size, which was selected based on previously published similar work from our laboratories. Animals were taken from multiple cages and breeding pairs.

Results

Lack of OCM expression causes early hearing loss in GCaMP6s adult mice

We utilized tissue-specific expression of GCaMP6s (Fig. 1A) to investigate Ca^{2+} signalling in the cochlea. *Atoh1*-driven Cre mice were crossed with the Ai96 mice containing a floxed-STOP cassette GCaMP6s. *Atoh1*
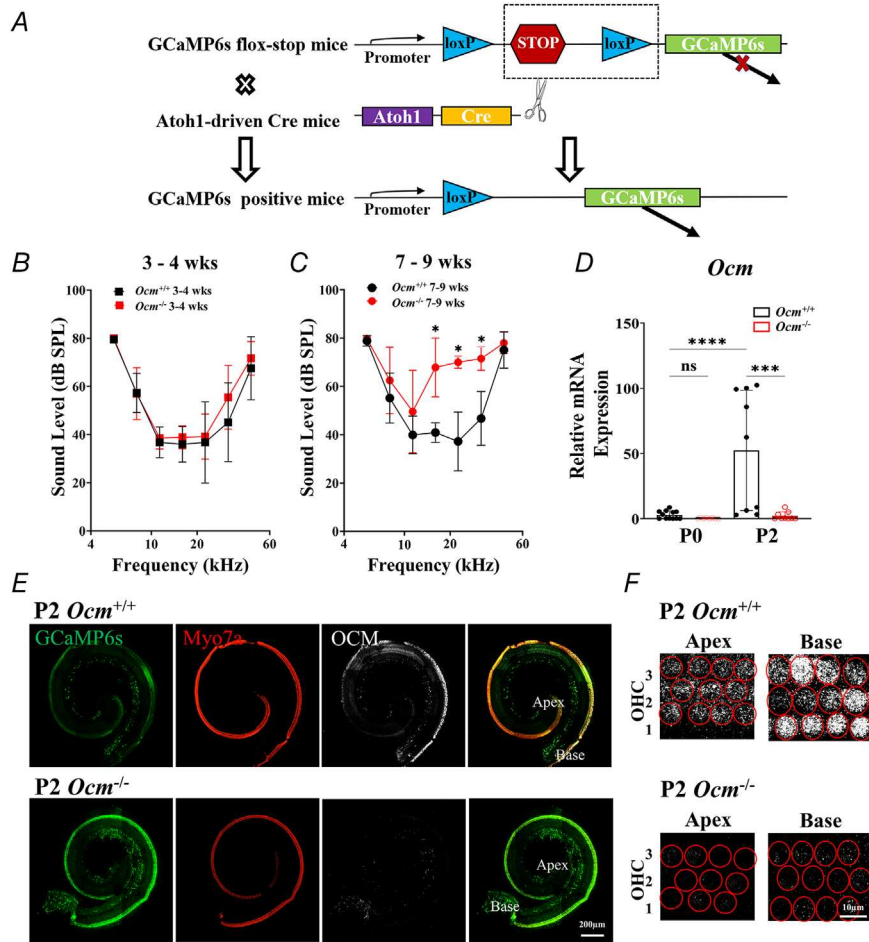
Figure 1. OCM expression in GCaMP6s mice can be detected as early as P2

A, schematic diagram showing generation of *Atoh1*-driven, GCaMP6s *Ocm*$^{+/+}$ and *Ocm*$^{-/-}$ mice. Ai96 mice (see Methods) contain a floxed-STOP cassette preventing transcription of the GCaMP6. After crossing with *Atoh1*-Cre mice, the floxed-STOP cassette was removed, leading to a tissue-specific expression of GCaMP6s in the inner ear region. *B* and *C*, distortion product otoacoustic emissions (DPOAEs) were measured from 3- to 4-week-old and 7- to 9-week-old *Ocm*$^{-/-}$ (8 and 5 mice, respectively) and aged-matched *Ocm*$^{+/+}$ mice (6 and 11 mice). For 3–4 weeks old, $P = 0.543$, two-way ANOVA, $P = 0.984$ at 5 kHz, $P > 0.999$ at 8 kHz, $P = 0.990$ at 11 kHz, $P = 0.980$ at 16 kHz, $P = 0.872$ at 22 kHz, $P > 0.999$ at 32 kHz, $P = 0.987$ at 45 kHz. For 7–9 weeks old, $P = 0.007$, two-way ANOVA, $P = 0.634$ at 5 kHz, $P = 0.982$ at 8 kHz, $P = 0.894$ at 11 kHz, $P = 0.017$ at 16 kHz, $P = 0.040$ at 22 kHz, $P = 0.020$ at 32 kHz, $P = 0.998$ at 45 kHz. *D*, qRT-PCR results of *Ocm* mRNA expression from the cochlea of *Ocm*$^{+/+}$ and *Ocm*$^{-/-}$ mice at postnatal day 0 (P0) and P2. Results are normalized to *Ocm*$^{+/+}$ at P0. $P < 0.001$, one-way ANOVA. $P > 0.999$ for P0 *Ocm*$^{+/+}$ *vs.* P0 *Ocm*$^{-/-}$, ***$P < 0.001$ for P2 *Ocm*$^{+/+}$ *vs.* P2 *Ocm*$^{-/-}$, ****$P < 0.0001$ for P0 *Ocm*$^{+/+}$ *vs.* P2 *Ocm*$^{+/+}$. Four and 3 *Ocm*$^{+/+}$ mice for P0 and P2, 3 *Ocm*$^{-/-}$ mice at both ages; 3 replicas for each animal group; no *Ocm* mRNA was detected from one of the P0 *Ocm*$^{-/-}$ replications. *E* and *F*, gradient expression of OCM along the tonotopic axis at P2. Maximum intensity projection images taken from the apical cochlea of *Ocm*$^{+/+}$ and *Ocm*$^{-/-}$ mice at P2. Cochleae showed endogenous green fluorescence (green). OCM (white) expression can be detected in P2 *Ocm*$^{+/+}$ mice, and exhibited a gradient expression along the cochlear coil, with a higher level at the base and lower at the apex ($n = 3$). Myo7a (red) was used as the hair cell marker.

expression is found in IHCs and OHCs during development (Mulvaney & Dabdoub, 2012). As a sensitive green fluorescent protein (GFP)-based Ca^{2+} sensor, GCaMP6s has been used to probe fast Ca^{2+} dynamics and low peak Ca^{2+} accumulations in neurons (Chen et al., 2013; Lukasz & Kindt, 2018; Shilling-Scrivo et al., 2021). Compared to other variants, GCaMP6 sensors have similar baseline fluorescence but a higher dynamic range (1.1- to 1.6-fold increase compared to GCaMP5G) and larger signals (>10-fold compared to GCaMP3) (Chen et al., 2013). Because of all the above features, we probed Ca^{2+} signalling in the OHCs using GCaMP6s *Ocm* control ($Ocm^{+/+}$) and *Ocm* knockout ($Ocm^{-/-}$) mice (Fig. 1A). Initially, we examined OHC function in adult *Ocm* mice expressing GCaMP6s by measuring distortion product otoacoustic emissions (DPOAEs). At 3–4 weeks, there were no differences in DPOAE thresholds between $Ocm^{+/+}$ and $Ocm^{-/-}$ mice (Fig. 1B). However, by 7–9 weeks, $Ocm^{-/-}$ mice showed hearing loss with higher DPOAE thresholds at 16, 22 and 32 kHz ($P = 0.007$, two-way ANOVA, Fig. 1C). These results are consistent with other studies showing that OCM is critical for maintaining cochlear function in adult mice (Climer et al., 2021; Tong et al., 2016).

In the cochlea of $Ocm^{+/+}$ mice, *Ocm* mRNA was detected as early as P0 and was significantly upregulated at P2. Relative *Ocm* mRNA expression in $Ocm^{-/-}$ cochlea was negligible compared to that of $Ocm^{+/+}$ (Fig. 1D, $P < 0.001$, one-way ANOVA). Using confocal microscopy, we found that at P2 both $Ocm^{+/+}$ and $Ocm^{-/-}$ mice showed endogenous GCaMP6s fluorescence in the cochlea (Fig. 1E). OHCs from $Ocm^{-/-}$ mice exhibited higher baseline fluorescence intensity compared to those in control mice (F_0, Fig. 1E), indicating a possible higher basal level of intracellular Ca^{2+} due to the lack of OCM as previously suggested (Murtha et al., 2022). OCM was also differentially expressed along the tonotopic axis of the cochlea, being higher towards the base of the cochlea (Fig. 1F).

The absence of OCM changes Ca^{2+} signalling in the postnatal development of $Ocm^{-/-}$ mice

Changes in intracellular Ca^{2+} induced by extracellular KCl caused increases in GCaMP6s fluorescence in OHCs (Fig. 2A, Movie 1), as previously demonstrated (Murtha et al., 2022). The change in Ca^{2+} levels in OHCs from all three rows was probed by the fractional change in signal fluorescence ($\Delta F/F_0$, Fig. 2B). OHCs from $Ocm^{-/-}$ mice showed significantly increased mean maximum $\Delta F/F_0$ compared $Ocm^{+/+}$ OHCs ($P < 0.001$, t test, Fig. 2C). The time course of the Ca^{2+} transient induced by extracellular KCl in $Ocm^{-/-}$ OHCs exhibited a faster rise-time constant compared to $Ocm^{+/+}$ OHCs at P2 (Fig. 2D). As a Ca^{2+}

binding protein, GCaMP6s could alter Ca^{2+} buffering in OHCs. However, GCaMP6s was present in OHCs from both control and $Ocm^{-/-}$ mice, and Ca^{2+} activity in $Ocm^{+/+}$ OHCs was similar to that previously measured in non-GCaMP6s transgenic mice (Murtha et al., 2022). We then sought to verify whether the KCl-induced Ca^{2+} transients depend on voltage-gated Ca^{2+} channels. In both $Ocm^{+/+}$ and $Ocm^{-/-}$ OHCs, Ca^{2+} transients were nearly eliminated when KCl was applied together with 250 μM nifedipine (Fig. 2E), and mean maximum $\Delta F/F_0$ was comparable in OHCs from both genotypes (maximum $\Delta F/F_0$ without normalization: 0.396 ± 0.175 for $Ocm^{+/+}$ mice, 0.448 ± 0.249 for $Ocm^{-/-}$ mice, $P = 0.153$, t test). A dose–response curve, normalized to $\Delta F/F_0$ with 250 μM nifedipine, showed that KCl-induced Ca^{2+} transients were partially blocked by 10 or 50 μM of the Ca^{2+} channel blocker ($P < 0.001$, two-way ANOVA, Fig. 2F). Since the $Ca_v1.3$ channel is the main voltage-gated L-type Ca^{2+} channel expressed in hair cells (Michna et al., 2003; Platzer et al., 2000), we investigated whether the lack of OCM altered their expression. qRT-PCR showed that the relative $Ca_v1.3$ mRNA expression (encoded by *CACNA1D*) in the cochlea of P2 $Ocm^{-/-}$ mice was significantly down-regulated compared to control mice ($P = 0.003$, t test, Fig. 2G). Western blot also showed that the $Ocm^{-/-}$ cochlea exhibited a significantly lower level of $Ca_v1.3$ protein compared to $Ocm^{+/+}$ cochlea ($P = 0.049$. t test, Fig. 2H and I).

Targeted deletion of *Ocm* increased spontaneous calcium signalling in the immature cochlea

During early postnatal development, OHCs show spontaneous Ca^{2+} activity that can be synchronized by ATP-induced Ca^{2+} waves originating from the GER, and depends on extracellular Ca^{2+} via $Ca_v1.3$ channel (Ceriani et al., 2019; Jeng et al., 2020). Since we recently showed that OCM expression alters intracellular Ca^{2+} signalling in OHCs (Murtha et al., 2022), we hypothesized that the absence of OCM in $Ocm^{-/-}$ mice could affect the spontaneous Ca^{2+} activity in the OHCs. Apical OHCs from both $Ocm^{+/+}$ and $Ocm^{-/-}$ P2 mice showed increased coordination of Ca^{2+} activity during the occurrence of a Ca^{2+} wave in the GER (time window 2, yellow), compared to when there were no Ca^{2+} waves (time window 1, green, Fig. 3A–F, Movie 2). Spontaneous Ca^{2+} activity was nearly eliminated in a Ca^{2+}-free medium (with 1 mM EGTA), and in the presence of 250 μM nifedipine, indicating that spontaneous Ca^{2+} activity in OHCs depends on extracellular Ca^{2+}. To quantify the synchronization of Ca^{2+} signals in OHCs with Ca^{2+} waves in the GER, the mean pairwise correlation coefficient between OHC Ca^{2+} traces was calculated in the time window during the occurrence of Ca^{2+} waves in the GER (r_{avg}). For

OHCs, the r_{avg} from both $Ocm^{+/+}$ and $Ocm^{-/-}$ mice showed a positive relationship with the longitudinal spread of Ca^{2+} events in the GER and was significantly different from zero (Fig. 4A, $P < 0.001$ for $Ocm^{+/+}$ and $Ocm^{-/-}$, *F*-test). There was no significant difference between the mean spread of Ca^{2+} waves in the GER from $Ocm^{+/+}$ and $Ocm^{-/-}$ mice ($Ocm^{+/+}$: 85.50 ± 61.00 μm,

$Ocm^{-/-}$: 95.90 ± 60.70 μm, $P = 0.193$, *t* test). These results indicate that the lack of OCM in OHCs did not change the positive relationship between the spread of Ca^{2+} waves in the GER and the correlation coefficient (Ceriani et al., 2019). Correlation coefficients displayed a monotonic relationship with the Ca^{2+} wave longitudinal spread. Fitting this relationship with linear regression
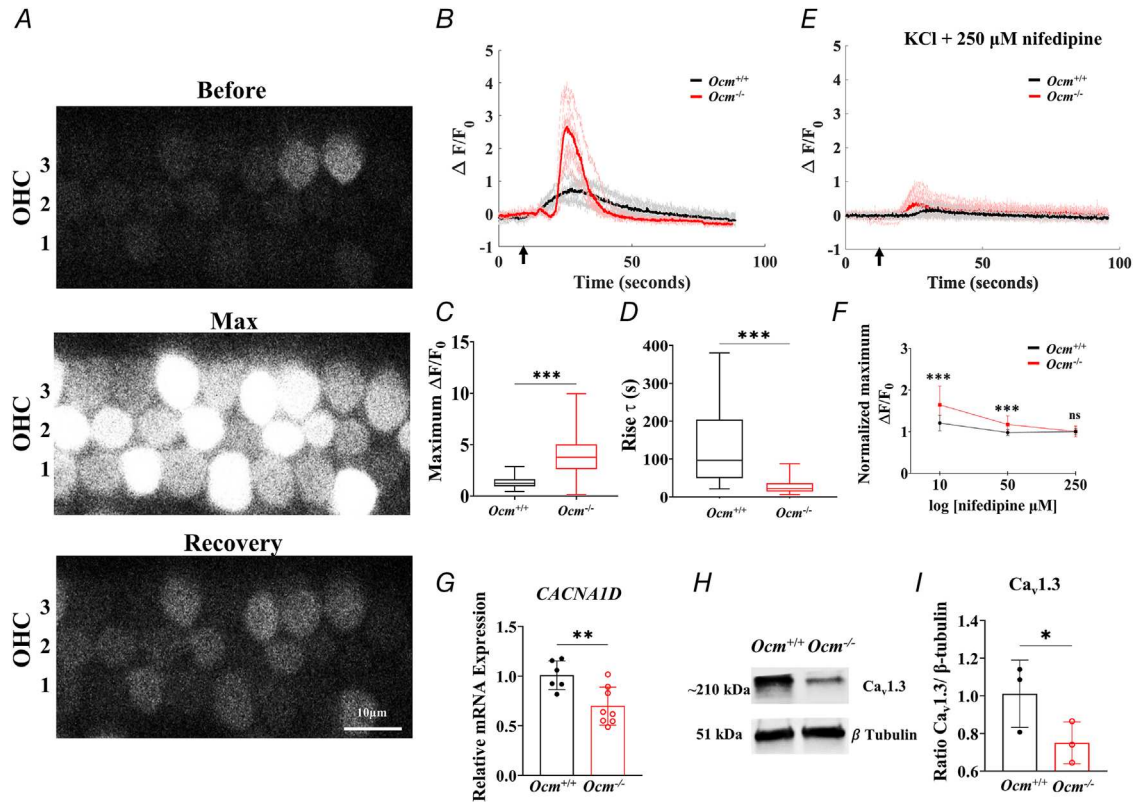
Figure 2. The absence of OCM increased the fractional change of voltage-gated Ca^{2+} influx in OHCs
A, organs of Corti were taken from GCaMP6s mice at P2. KCl (37 mM final concentration) superfusion was administered to elicit Ca^{2+} transients. GCaMP6s fluorescence is shown before the superfusion of KCl (top), at peak response (middle) and the recovery stage (bottom). Recordings were taken at room temperature ($\sim$24°C). Representative Ca^{2+} transient images taken from the cochlear apex of $Ocm^{-/-}$ P2 mice. *B*, representative plots of GCaMP6s fluorescence fractional change ($\Delta F/F_0$) in OHCs induced by KCl superfusion (arrow). Results show individual ROI fluorescence $\Delta F/F_0$ trace view (grey and light red) and mean $\Delta F/F_0$ for OHCs (black and red) from P2 $Ocm^{+/+}$ and $Ocm^{-/-}$ mice. *C*, average maximum fluorescence intensities from OHCs of P2 $Ocm^{+/+}$ and $Ocm^{-/-}$ mice during the application of KCl. Mean peak $\Delta F/F_0$ values are plotted from single OHCs in all 3 rows (39 OHCs from 4 $Ocm^{+/+}$ mice, 208 OHCs from 6 $Ocm^{-/-}$, $P < 0.001$, *t* test). *D*, rise τ from OHCs of P2 $Ocm^{+/+}$ and $Ocm^{-/-}$ mice during the application of KCl (20 OHCs from 4 $Ocm^{+/+}$ mice, 73 OHCs from 6 $Ocm^{-/-}$ mice, $P < 0.001$, Mann–Whitney test). *E*, individual $\Delta F/F_0$ traces (grey and light red) and mean $\Delta F/F_0$ (black and red) from $Ocm^{+/+}$ and $Ocm^{-/-}$ OHCs induced by the KCl application (arrow) with the presence of 250 μM nifedipine. *F*, normalized maximum $\Delta F/F_0$ showing the effect of nifedipine on KCl-induced Ca^{2+} transients in OHCs from $Ocm^{+/+}$ and $Ocm^{-/-}$ P2 mice. Cochlear explants were incubated with 10, 50 and 250 μM nifedipine before KCl perfusion. Relative peak $\Delta F/F_0$ values from different nifedipine dosage treatments were normalized to mean peak $\Delta F/F_0$ when 250 μM nifedipine was applied. *x*-Axis: logarithm of nifedipine concentration. ***$P < 0.001$, two-way ANOVA, $P < 0.001$ for 10 μM nifedipine, 43 OHCs from 2 $Ocm^{+/+}$ and 68 OHCs from 2 $Ocm^{-/-}$ mice; $P < 0.001$ for 50 μM nifedipine, 34 OHCs from 2 $Ocm^{+/+}$ and 95 OHCs from 2 $Ocm^{-/-}$ mice; $P > 0.999$ for 250 μM nifedipine, 28 OHCs from 2 $Ocm^{+/+}$ and 81 OHCs from 2 $Ocm^{-/-}$ mice. *G*, qRT-PCR results of $Ca_v1.3$ (*CACNA1D*), 6 replicas from 3 $Ocm^{+/+}$ and 8 replicas from 3 $Ocm^{-/-}$ mice at P2. Plots are normalized mRNA levels relative to $Ocm^{+/+}$, $P = 0.003$, *t* test. *H* and *I*, representative western blot for $Ca_v1.3$ protein expression levels detected in cochlea harvested from P2 $Ocm^{+/+}$ and $Ocm^{-/-}$ mice. Each genotype has $n = 3$ independent repeats, each replicate contained 3 cochleae, total animal $n = 9$ for each genotype. *$P = 0.049$, *t* test. β-Tubulin (loading control) was used for normalization. The plot is normalized grey values relative to P2 $Ocm^{+/+}$ mice.

yielded a steeper slope for $Ocm^{-/-}$ compared to $Ocm^{+/+}$ (4.39 ± 0.93 *vs.* 2.66 ± 0.88/nm, $P = 0.008$, *t* test, Fig. 4A). We calculated the mean r_{avg} in OHCs; $Ocm^{-/-}$ OHCs exhibited a significantly increased mean r_{avg} compared to $Ocm^{+/+}$ OHCs ($P = 0.006$, Mann–Whitney test, Fig. 4B). We then calculated the mean maximum $\Delta F/F_0$ for each Ca^{2+} spike in OHCs (Fig. 4C and D). During spontaneous Ca^{2+} waves, the mean maximum $\Delta F/F_0$ in $Ocm^{-/-}$ OHCs was greater than in $Ocm^{+/+}$ OHCs (Fig. 4D, $P < 0.001$, Mann–Whitney test). Altogether, we found that similar-sized Ca^{2+} waves from the GER produced increased synchronization and higher mean maximum $\Delta F/F_0$ of spontaneous Ca^{2+} activity in the OHCs of $Ocm^{-/-}$ relative to those in $Ocm^{+/+}$ mice.

Lack of OCM expression increases ATP-induced Ca^{2+} signalling in cochlear OHCs

ATP signalling plays a central role during the development of the cochlea. Cochlear cells exhibit a diverse array of purinergic signalling components including all subtypes of ionotropic P2X and metabotropic P2Y receptor subunits (Housley et al., 2009). In the immature

cochlea, OHCs express P2X and P2Y receptors and exhibit depolarizing, ATP-gated currents (Bobbin, 2001; Glowatzki et al., 1997). Initially, we investigated whether purinergic signalling is altered in the absence of OCM, by investigating whether spontaneous Ca^{2+} activity in OHCs was blocked by the ionotropic P2X purinergic receptor antagonist PPADS (100 μM). Both $Ocm^{+/+}$ and $Ocm^{-/-}$ OHCs showed spontaneous Ca^{2+} activity (Fig. 5A and C). However, in the presence of PPADS, the Ca^{2+} waves originating from the GER failed to synchronize the Ca^{2+} signalling in OHCs (Fig. 5B and D, time window 1 *vs.* time window 2). The presence of PPADS also affected the linear relationship between the spread of Ca^{2+} waves in GER and the r_{avg} in both $Ocm^{+/+}$ and $Ocm^{-/-}$ OHCs (Fig. 5E). However, the mean maximum $\Delta F/F_0$ of spontaneous spikes was significantly decreased only in $Ocm^{-/-}$ OHCs (Fig. 5G, $P < 0.001$, two-way ANOVA).

The absence of OCM upregulates purinergic receptors expression in OHCs

We then investigated whether Ca^{2+} transients in OHCs elicited by extracellular ATP were affected in the absence

Figure 3. Ca^{2+} waves initiated from the GER synchronized spontaneous Ca^{2+} activities in $Ocm^{+/+}$ and $Ocm^{-/-}$ OHCs
A and D, apical coil of the cochleae taken from GCaMP6s mice at P2. Individual ROI GCaMP6s fluorescence intensity is shown as fractional change ($\Delta F/F_0$) traces for all OHCs from a single field of view (black), and Ca^{2+} activity in GER (red). Highlighted green time window (1) represents no Ca^{2+} wave in GER. In contrast, the yellow time window (2) marks the occurrence of a Ca^{2+} wave in GER. Recordings were taken at ~24°C. B and E, representative images taken from time windows 1 (green) and 2 (yellow) showing the background and the occurrence of the Ca^{2+} waves in GER for $Ocm^{+/+}$ and $Ocm^{-/-}$ cochlea, respectively. Dash lines represent the spread (extension size) of the Ca^{2+} wave in GER along the cochlear spiral. C and F, representative correlation matrices of $\Delta F/F_0$ traces in OHCs. Correlation matrices were computed during time window 1 (top panel), and time window 2 (bottom panel). Each matrix element represents Spearman's rank correlation coefficient (r_S, see Methods) of one pair of OHCs from the same cochlear spiral.
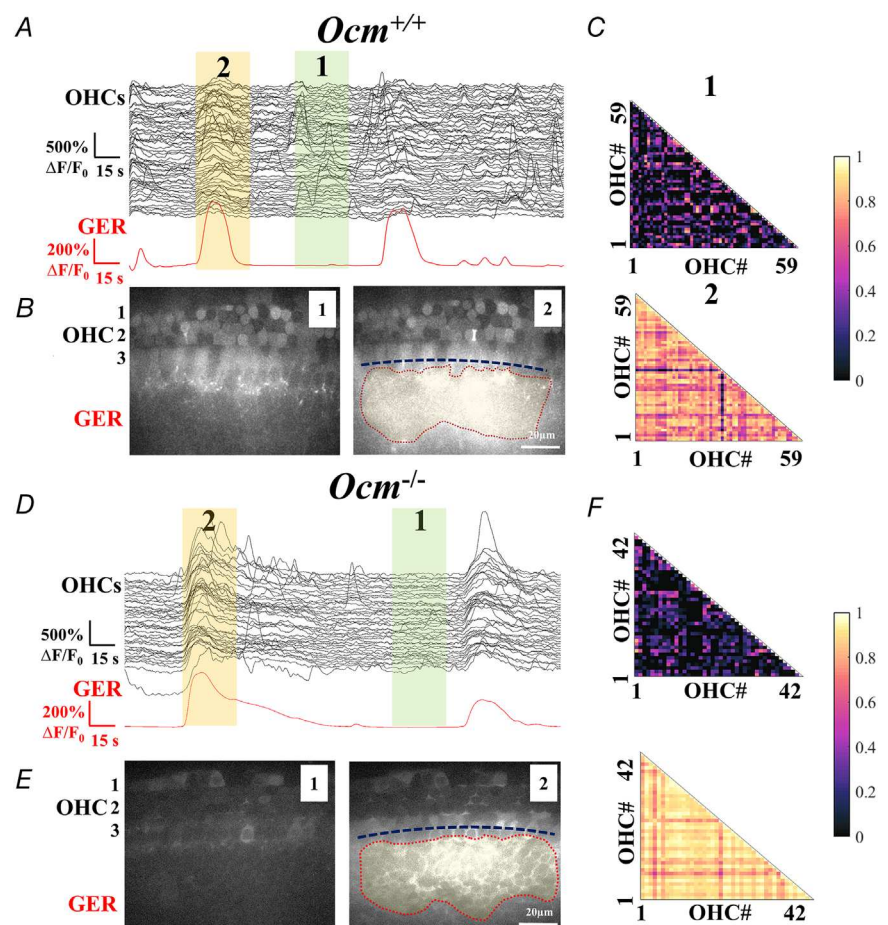
of OCM at P2. $Ocm^{-/-}$ OHCs showed significantly higher maximum $\Delta F/F_0$ signal compared to $Ocm^{+/+}$ mice (Movie 3, Fig. 6A–C, $P < 0.001$, t test). ATP-induced Ca^{2+} transients in $Ocm^{-/-}$ OHCs were nearly eliminated in Ca^{2+}-free medium (with 1 mM EGTA, the mean of maximum $\Delta F/F_0$: 0.664 ± 0.495, 43 OHCs from 2 mice). The Ca^{2+} activity was abolished in OHCs when ATP was applied with the presence of 100 μM PPADS (the mean of maximum $\Delta F/F_0$: 0.351 ± 0.142, 35 OHCs from 2 mice). Altogether, these data indicate that purinergic signalling can modulate spontaneous Ca^{2+} activity in both $Ocm^{+/+}$ and $Ocm^{-/-}$ OHCs. Since the lack of OCM causes a larger Ca^{2+} response induced by ATP in OHCs similar to KCl, we investigated whether there were changes in the expression of P2X receptors. Among known P2X receptors, P2X2, P2X3 and P2X7 are all expressed in the cochlea during development (Housley et al., 1998; Huang et al., 2006; Nikolic et al., 2003). We performed qRT-PCR on cochlea harvested from $Ocm^{+/+}$ and $Ocm^{-/-}$ mice at P2. *P2RX2*, *P2RX3* and *P2RX7* mRNA expression

was significantly higher in $Ocm^{-/-}$ cochlea compared to $Ocm^{+/+}$ cochlea (Fig. 7A; *P2RX2*, $P = 0.021$; *P2RX3*, $P < 0.001$; and *P2RX7*, $P = 0.028$; t test). However, *P2RX2* receptor expression demonstrated the greatest fold change among the three purinergic receptors (>10-fold) in OHCs from $Ocm^{-/-}$ mice compared with littermate controls. Western blot revealed that $Ocm^{-/-}$ cochlea showed significantly upregulated P2X2 protein expression relative to $Ocm^{+/+}$ (Fig. 7B, $P = 0.026$, t test), which was further supported by immunofluorescence experiments (Fig. 7C).

The number of afferent fibres in $Ocm^{-/-}$ mice is increased

In the cochlea, the type II afferent fibres cross the tunnel and contact multiple OHCs, and form branches to the outer supporting cells, including Deiter's cells and Hensen's cells (Fechner et al., 2001). The maturation of
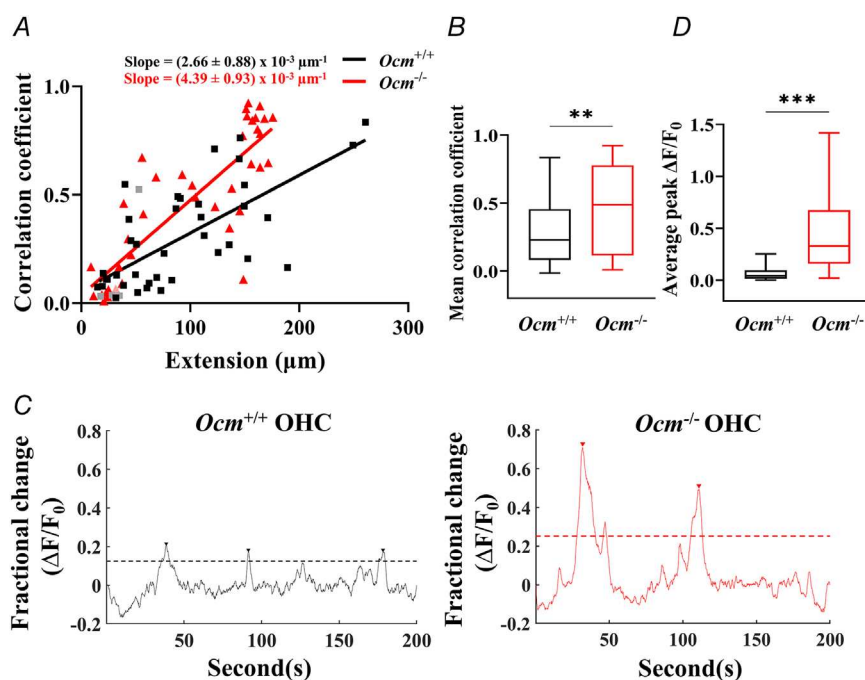

Figure 4. $Ocm^{-/-}$ OHCs exhibited a higher level of correlated Ca^{2+} activity and increased maximum $\Delta F/F_0$ during the Ca^{2+} waves initiated in the GER

A, the linear regression between the longitudinal spread (extension) of spontaneous Ca^{2+} waves in GER and the mean Spearman's rank correlation coefficient (r_{avg}, see Methods) of OHCs from $Ocm^{+/+}$ and $Ocm^{-/-}$ apical cochlea. Black and red symbols represent a significant increase in pairwise OHC correlation ($P < 0.050$, Mann–Whitney U-test) compared to their background time window. Grey and light red symbols represent that the correlation did not increase significantly. The slope rates are shown and were significantly different from zero ($P < 0.001$ for both $Ocm^{+/+}$ and $Ocm^{-/-}$ OHCs, F-test). $Ocm^{+/+}$: 44 Ca^{2+} waves, 11 cochleae and 8 mice; $Ocm^{-/-}$: 42 Ca^{2+} waves, 11 cochleae and 6 mice. *B*, mean correlation coefficient between the spread (extension size) of Ca^{2+} wave in GER and the r_{avg} in OHCs during the Ca^{2+} waves calculated from above. ns: no significance, **$P = 0.006$, Mann–Whitney test. Number of waves, cochleae and mice as listed in panel *A*. *C*, representative Ca^{2+} signalling in single OHC from $Ocm^{+/+}$ and $Ocm^{-/-}$ apical cochleae. Arrow represents a Ca^{2+} spike in OHC and only spikes that exceeded the threshold (dash line) were measured (see Methods). *D*, mean maximum $\Delta F/F_0$ of OHC spontaneous Ca^{2+} activity. ***$P < 0.001$, Mann–Whitney test. $Ocm^{+/+}$: 2171 Ca^{2+} spikes in OHCs from 11 cochleae; $Ocm^{-/-}$: 2198 Ca^{2+} spikes in OHCs from 11 cochleae.

synaptic contacts includes a transformation from multiple small to one single presynaptic active zone (Michanski et al., 2019). Thus, we expected that the changes in spontaneous Ca^{2+} activity might affect ribbon synapse maturation and afferent innervation in $Ocm^{-/-}$ OHCs. We first counted the number of afferent ribbons in OHCs from pre- and post-hearing $Ocm^{+/+}$ and $Ocm^{-/-}$ mice. The number of CtBP2 puncta in OHCs increased between P2 and P6 in both $Ocm^{+/+}$ and $Ocm^{-/-}$ mice. Between P6 and P10 there was a drastic reduction of puncta in $Ocm^{+/+}$ mice, but not in $Ocm^{-/-}$ mice. However, by

3–4 weeks, the number of ribbons labelled by CtBP2 in $Ocm^{+/+}$ and $Ocm^{-/-}$ apical cochlea showed no significant difference (Fig. 8A–E, $P = 0.004$, two-way ANOVA). Our results suggested that the synaptic maturation and pruning in $Ocm^{-/-}$ cochlea was delayed compared to $Ocm^{+/+}$ cochlea. We then used peripherin to examine type II afferent spiral ganglion (SG) fibres (Hafidi, 1998) in cochleae from $Ocm^{+/+}$ and $Ocm^{-/-}$ mice at P6 and P10 (Fig. 9A and B). The SG neurons formed outer spiral fibres that terminate on OHCs after long spiral courses. Peripherin immunofluorescence revealed that $Ocm^{-/-}$
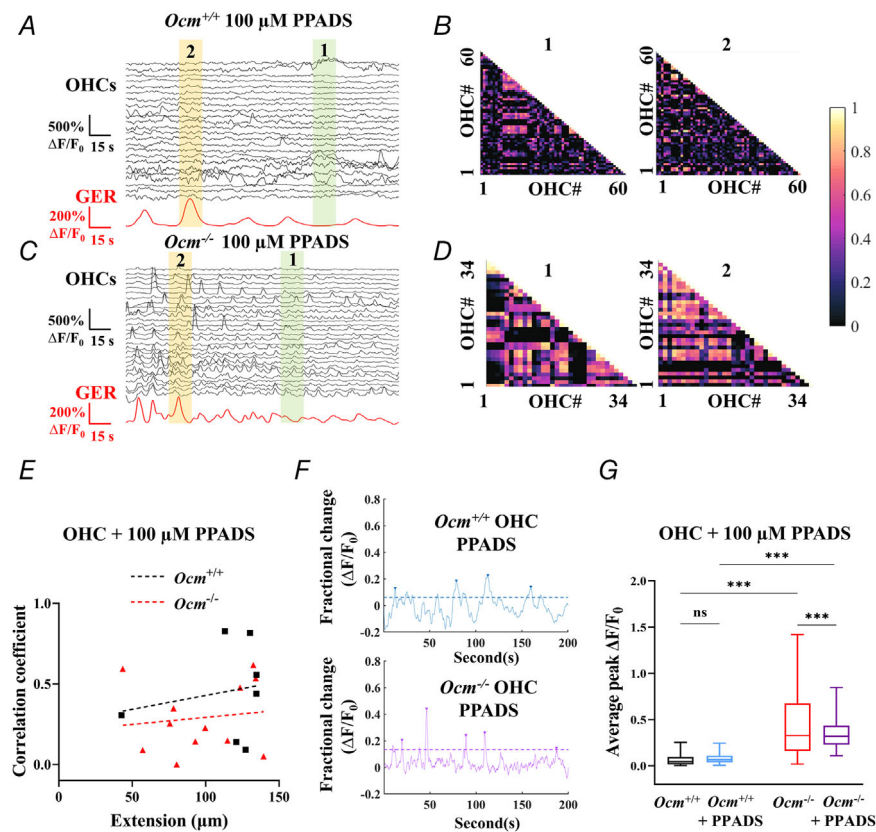
Figure 5. The purinergic receptor is required for the synchronization of spontaneous Ca^{2+} activity

A–D, individual ROI $\Delta F/F_0$ traces for all OHCs from a single field of view (black) and Ca^{2+} activity in GER (red) were taken from $Ocm^{+/+}$ and $Ocm^{-/-}$ mice at P2. Highlighted green (1) and yellow (2) time windows represent no Ca^{2+} wave (background), and the occurrence of Ca^{2+} wave in GER, respectively, and were used for correlation analysis. The right panel shows representative Ca^{2+} signalling in a single OHC. *B* and *D*, representative correlation matrices calculated from *A* and *C* time window 1 (background, left panel) and time window 2 (during the occurrence of Ca^{2+} wave in GER, right panel). Each matrix element represents Spearman's rank correlation coefficient (r_S) of one pair of OHCs. *E*, the linear regression between the longitudinal spread (extension) of spontaneous Ca^{2+} waves in GER and the mean Spearman's rank correlation coefficient (r_{avg}, see Methods) of OHCs from $Ocm^{+/+}$ and $Ocm^{-/-}$ apical cochlea with the continuous presence of PPADS (100 μM). $Ocm^{+/+}$: 7 waves from 4 mice; $Ocm^{-/-}$: 12 waves from 3 mice. The slope from both $Ocm^{+/+}$ and $Ocm^{-/-}$ OHC showed no significant deviation from zero ($Ocm^{+/+}$: $P = 0.685$, $Ocm^{-/-}$: $P = 0.695$, *F*-test). *F* and *G*, representative Ca^{2+} signalling in single OHC from $Ocm^{+/+}$ and $Ocm^{-/-}$ apical cochlea with the presence of PPADS (100 μM). Arrow represents a Ca^{2+} spike in OHC; only spikes that exceeded the threshold (dash line) were calculated (see Methods). The mean maximum $\Delta F/F_0$ of OHCs spontaneous Ca^{2+} activity with the presence or absence of PPADS was plotted. $P < 0.001$, two-way ANOVA. ns $P = 0.651$ for $Ocm^{+/+}$ with or without PPADS, ***$P < 0.001$ for $Ocm^{-/-}$ with or without PPADS, ***$P < 0.001$ for $Ocm^{+/+}$ with PPADS and $Ocm^{-/-}$ with PPADS (3 mice for each genotype, 560 spikes from $Ocm^{+/+}$ OHCs and 588 spikes from $Ocm^{-/-}$ OHCs).

mice showed a similar number of tunnel crossing fibres compared to $Ocm^{+/+}$ mice at P6 (Fig. 9C), but had an increased number of tunnel crossing fibres compared to $Ocm^{+/+}$ mice at P10 (Fig. 9D, $P = 0.002$, t test). These data provide evidence that the increased spontaneous Ca^{2+} signalling in $Ocm^{-/-}$ cochlea changes the maturation of afferent synapses and innervation of afferent fibres during development.
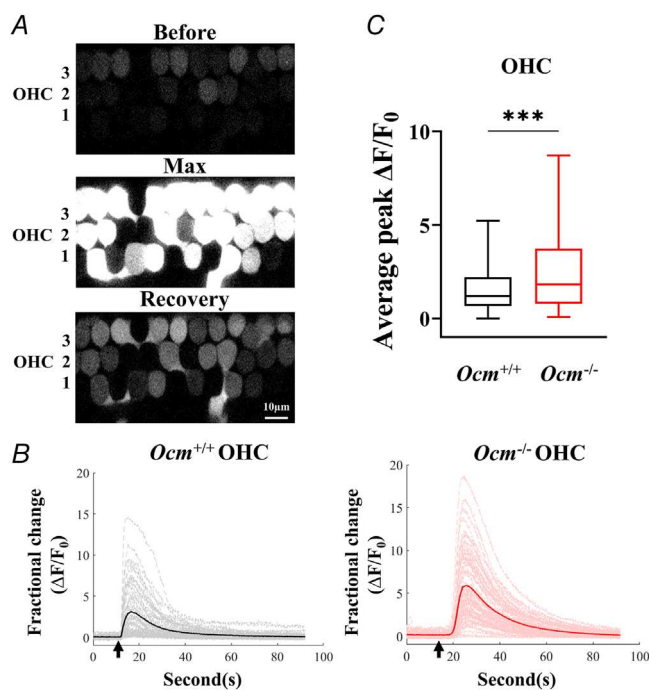
Discussion

In the present study, we showed that OCM influences the development of spontaneous activity in OHCs and modulates their neonatal afferent innervation. We generated $Ocm^{+/+}$ and $Ocm^{-/-}$ mice with a genetically encoded calcium sensor (GCaMP6s). Similar to other studies (Climer et al., 2021; Tong et al., 2016), $Ocm^{-/-}$ mice showed normal hearing at 3–4 weeks of age but exhibited an early onset hearing loss at 7–9 weeks. Compared to $Ocm^{+/+}$ mice, OHCs from P2 $Ocm^{-/-}$ mice

Figure 6. ATP-induced Ca^{2+} transients are altered in $Ocm^{-/-}$ mice
A, representative images of Ca^{2+} transients in OHCs from P2 $Ocm^{-/-}$ mice shown before 200 μM ATP superfusion, at peak response, and the recovery stage. *B*, representative plots of the fractional change ($\Delta F/F_0$) in GCaMP6s fluorescence induced by 200 μM ATP superfusion (arrow). Results show individual ROI fluorescence $\Delta F/F_0$ trace view (grey and light red) and mean $\Delta F/F_0$ for OHCs from P2 $Ocm^{+/+}$ and $Ocm^{-/-}$ mice. *C*, mean maximum $\Delta F/F_0$ of OHCs from $Ocm^{+/+}$ and $Ocm^{-/-}$ mice at P2, induced by 200 μM ATP superfusion. ***$P < 0.001$, Mann–Whitney test, 119 OHCs from 4 $Ocm^{+/+}$ mice, 325 OHCs from 7 $Ocm^{-/-}$ mice.

have higher maximum $\Delta F/F_0$ GCaMP6s fluorescence intensity induced by ATP and KCl, which is consistent with higher levels of free cytosolic Ca^{2+} as previously reported (Murtha et al., 2022). Both $Ocm^{+/+}$ and $Ocm^{-/-}$ OHCs exhibited spontaneous Ca^{2+} activity that is synchronized by Ca^{2+} waves initiated from the GER. However, OHCs from $Ocm^{-/-}$ mice had an increased level of coordinated spontaneous Ca^{2+} activity compared to littermate controls. Further, $Ocm^{-/-}$ OHCs exhibited an increased number of presynaptic ribbons and afferent tunnel-crossing fibres just prior to the onset of hearing. Taken together OCM contributes to the modulation of Ca^{2+} signalling and the maturation of afferent connectivity in the developing mouse cochlea.

OCM modulates the expression of Ca^{2+}-related genes during development

Purinergic receptors have been implicated in auditory neurotransmission, regulation of cochlear homeostasis, cochlear development and neurodegenerative conditions (Burnstock, 2016; Housley et al., 2009; Linden et al., 2019). Previous studies have shown that all P2X receptors are transiently expressed in the developing mammalian cochlea (Vlajkovic & Thorne, 2022). Among these purinergic receptors, P2X3 and P2X7 are expressed in sensory hair cells from embryonic day 18 (E18) to P6 (Huang et al., 2006; Nikolic et al., 2003). P2X2 receptors are the predominant purinergic receptor in the mature cochlea and are expressed in hair cells before P15 (Jarlebark et al., 2002). We found that the expression of P2X2, P2X3 and P2X7 purinergic receptors was upregulated due to the lack of OCM. The upregulation of P2X receptors in the $Ocm^{-/-}$ cochlea could be explained either by an OCM-mediated regulatory pathway or by the effect of Ca^{2+} levels on purinergic reveptor expression. Several studies suggest CaBPs may interact directly with purinergic receptors. Roger et al. (2008) found that P2X7 receptors contain a large intracellular C-terminal domain with a Ca^{2+}-dependent calmodulin (CaM) binding motif. Moreover, the Ca^{2+}–CaM binding motif changes the conformation of P2X7, indicating a possible intracellular regulatory pathway of P2X7 receptors (Sander et al., 2022). Since OCM and CaM share some functional similarities (Climer et al., 2019; MacManus et al., 1982), it is possible that OCM may interact with P2X receptors to alter their function and expression. Alternatively, upregulated purinergic receptors could be associated with the higher concentrations of cytosolic free Ca^{2+} in $Ocm^{-/-}$ OHCs. Loss of OCM or noise exposure has been shown to cause increased levels of intracellular free Ca^{2+}, leading to Ca^{2+} overloading in OHCs (Murtha et al., 2022; Zuo et al., 2008). Noise exposure also leads to the upregulation of P2X receptors in sensory hair cells (Wang et al., 2003).

Thus, the loss of OCM could lead to unrestrained P2X function and increased expression either because of the loss of a direct regulator, or through unfettered cytosolic free Ca^{2+}.

Unlike the upregulation of P2X receptors, we found that the expression of $Ca_v1.3$, which is the predominant voltage-gated Ca^{2+} channel in hair cells (Hafidi & Dulon, 2004; Michna et al., 2003), was downregulated in the $Ocm^{-/-}$ cochlea. Spontaneous Ca^{2+} activity in OHCs is dependent upon the expression of $Ca_v1.3$ channels (Ceriani et al., 2019; Jeng et al., 2020). Although there is little evidence for CaBPs directly modulating $Ca_v1.3$ expression, previous studies show that CaBPs can modulate $Ca_v1.3$ activity. CaM modulates $Ca_v1.3$ channel open probability based on cytosolic Ca^{2+} levels (Johny et al., 2013). CaM increases the activity of $Ca_v1.3$ channels at low cytosolic Ca^{2+} levels, and decreases the permeability of $Ca_v1.3$ channels at high Ca^{2+} levels. Additionally, other CaBPs (e.g. CaBP1, CaBP2, CaBP3 and CaBP4) enhance Ca^{2+} feedback to $Ca_v1.3$ channels (Cui et al., 2007). Similar to other CaBPs, OCM could potentially modulate the function of $Ca_v1.3$ channels. In this way, the expression of OCM or the downregulation of Ca^{2+} entry prevents Ca^{2+} overloading in OHCs and protects them from cytotoxicity. Indeed, mice lacking

$Ca_v1.2$, another voltage-gated Ca^{2+} channel expressed in hair cells, have reduced vulnerability to noise (Zuccotti et al., 2013). The progressive hearing loss phenotype observed in $Ocm^{-/-}$ mice could be the result of the insufficiency of protective mechanisms in $Ocm^{-/-}$ OHCs to reduce intracellular Ca^{2+} and thus protect mice from hearing loss.

Taken together, our data suggest that OCM regulates the expression of two purinergic receptors and $Ca_v1.3$ channels during the early stages of development. Therefore, OCM may contribute significantly to shaping Ca^{2+} dynamics, a cornerstone of auditory hair cell function. Since noise leads to changes in Ca^{2+} activity and Ca^{2+}-related gene expression, OCM could play a key role in preventing OHC damage due to noise exposure.

Lack of OCM alters spontaneous Ca^{2+} activity and afferent maturation in OHCs

Our data show that OHCs from pre-hearing $Ocm^{-/-}$ mice exhibited higher synchronized Ca^{2+} activity compared to OHCs from littermate control mice. Spontaneous Ca^{2+} waves are generated from the GER and travel to the lesser epithelial ridge (LER), where the OHCs are located. Deiters' cells in LER synchronize the Ca^{2+} activity in


Figure 7. P2X purinoceptor 2 (P2X2) expression is upregulated in $Ocm^{-/-}$ mice
A, qRT-PCR results show that *P2RX2*, *P2RX3* and *P2RX7* relative expression level is significantly increased in the cochlea of P2 $Ocm^{-/-}$ mice compared to littermate controls. For *P2RX2*, 9 replicas from 3 animals for each genotype. For *P2RX3* and *P2RX7*, 9 replicates from 3 animals for $Ocm^{+/+}$, 12 replicates from 4 animals for $Ocm^{-/-}$. All values were normalized to $Ocm^{+/+}$. *P = 0.021 for *P2RX2*, ***P < 0.001 for *P2RX3*, *P = 0.028 for *P2RX7*. *B*, representative western blot for P2X2 expression levels detected in cochlea derived from P2 $Ocm^{+/+}$ and $Ocm^{-/-}$ mice. β-Tubulin (loading control) was used for normalization. Two replicates for $Ocm^{+/+}$, 3 replicates for $Ocm^{-/-}$, each one containing 3 mice cochlear spirals. Plot is normalized grey values relative to $Ocm^{+/+}$. *P = 0.026, *t* test. *C*, maximum intensity projections of P2X2 immunolabelling on three rows of OHCs harvested from P2 $Ocm^{+/+}$ and $Ocm^{-/-}$ mice; n = 3 for each genotype. P2X2 (white), and GCaMP6s (green) are shown.
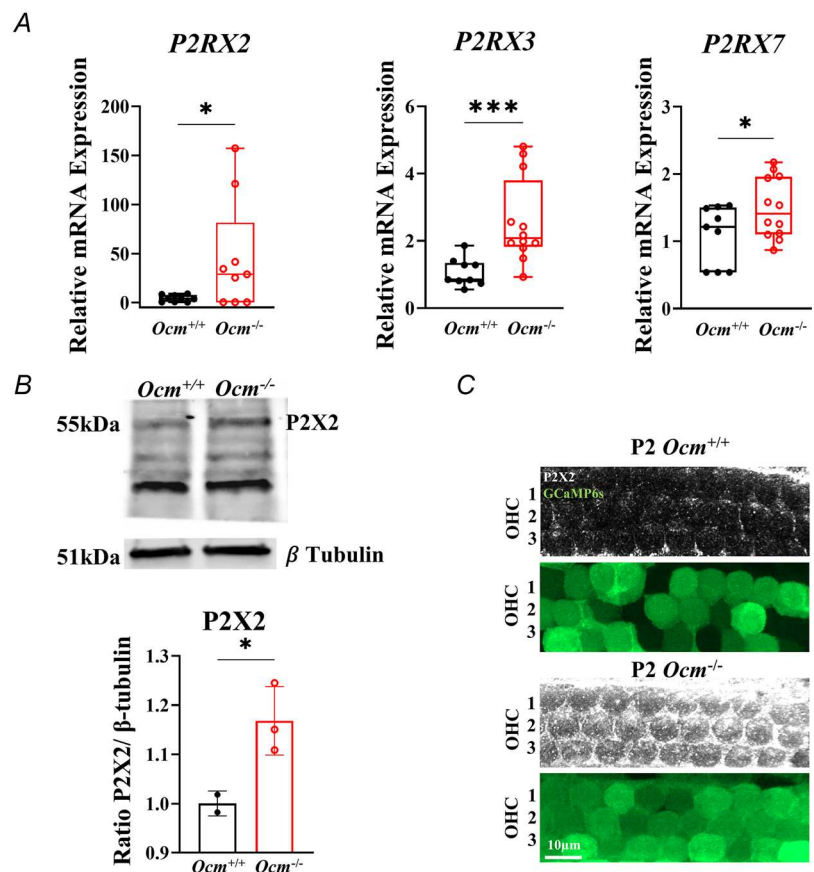
nearby OHCs via the release of ATP (Ceriani et al., 2019). Interestingly, the expression of OCM in OHCs increases during development (Hackney et al., 2005; Simmons et al., 2010), and parallels the downregulation of spontaneous Ca^{2+} activity in developing OHCs (Ceriani et al., 2019; Jeng et al., 2020). In the present study, we found a gradient expression of OCM in OHCs along the tonotopic axis of the cochlea. Indeed, spontaneous Ca^{2+} activity is higher in apical compared to basal OHCs at early postnatal ages (Ceriani et al., 2019; Jeng et al., 2020; Lelli et al., 2009). These studies support the idea that OCM regulates spontaneous Ca^{2+} activity during the maturation of OHCs. Both $Ca_v1.3$ Ca^{2+} channels and purinergic receptor channels are thought to modulate spontaneous Ca^{2+} activity in developing OHCs. We found the lack of OCM downregulates the $Ca_v1.3$ expression, but upregulates the ATP receptor expression. In OHCs

from $Ocm^{-/-}$ mice, the larger Ca^{2+} transients during spontaneous Ca^{2+} activity in OHCs is due, at least partly, to the upregulation of ATP receptors, while the downregulation of $Ca_v1.3$ could be a compensatory mechanism of Ca^{2+} overloading caused by the lack of OCM.

During the early postanal period, Ca^{2+} influxes and periodic Ca^{2+} stimulation are required for synaptic maturation and afferent refinement (Balland et al., 2006; Sheets et al., 2012; Spitzer, 2006; Tritsch et al., 2007). Recent studies suggest that coordinated Ca^{2+} activity in OHCs is necessary for the formation of their afferent connectivity. The reduction of synchronized spontaneous Ca^{2+} activity in the connexin 30 knockout ($Cx30^{-/-}$) OHCs results in a decreased number of ribbon synapses and type II afferent fibres (Ceriani et al., 2019; Jeng et al., 2020). Here, we found that a higher level of spontaneous Ca^{2+} activity increases the number of synaptic ribbons
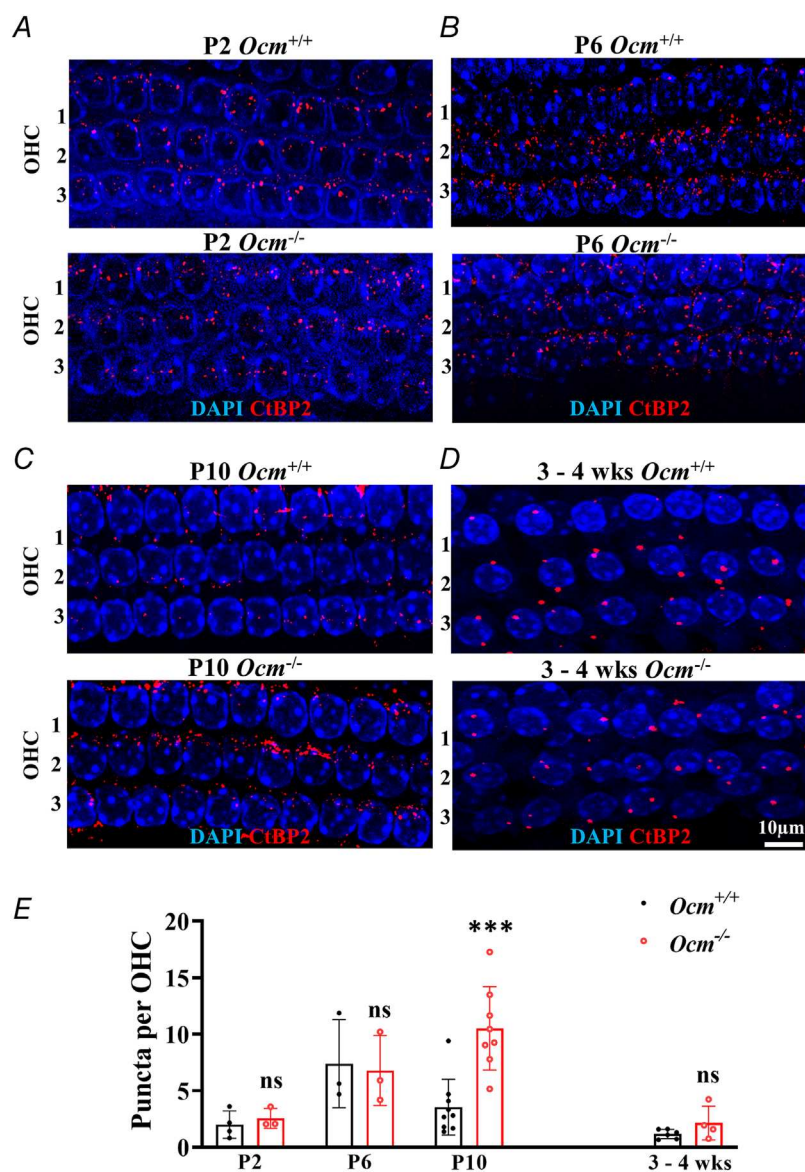
Figure 8. Ribbon synapse maturation is delayed in $Ocm^{-/-}$ mice

A–D, maximum intensity projections of confocal *z*-stacks from $Ocm^{+/+}$ and $Ocm^{-/-}$ apical cochlea at P2, P6, P10 and 3–4 weeks. Three rows of OHCs with ribbon synapses (CtBP2, red) and DAPI (blue) are shown. *E*, the mean number of ribbon synapses puncta per OHC from the apical cochlea was measured. The CtBP2 puncta within 4 μm of the OHC nuclei were counted. Bar graphs show the number of ribbons per OHC. $P = 0.004$, two-way ANOVA. At P2, ns $P > 0.999$, 4 $Ocm^{+/+}$ and 3 $Ocm^{-/-}$ mice. At P6, ns $P > 0.999$, 3 $Ocm^{+/+}$ and 3 $Ocm^{-/-}$ mice. At P10, ***$P < 0.001$, 9 $Ocm^{+/+}$ and 8 $Ocm^{-/-}$ mice. At 3–4 weeks, ns $P > 0.999$, 6 $Ocm^{+/+}$ and 4 $Ocm^{-/-}$ mice.
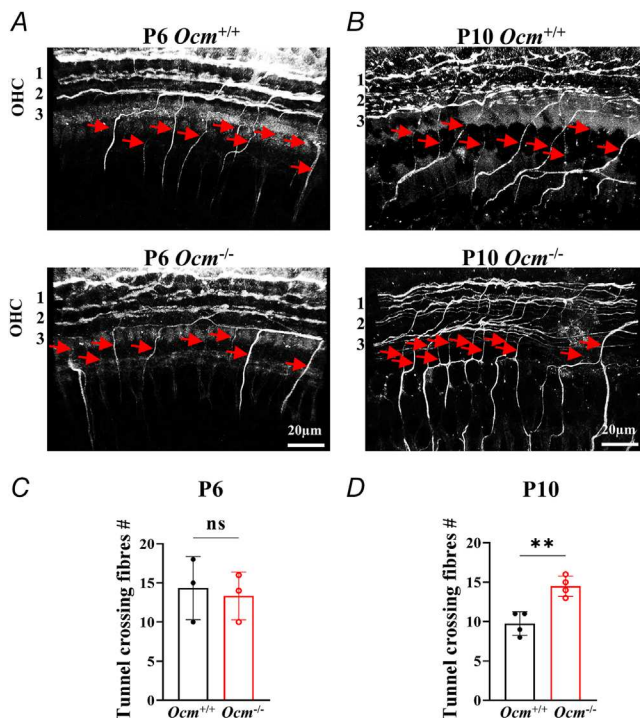
and type II afferent fibres. These data reveal that similar to $Cx30^{-/-}$, OCM-regulated spontaneous Ca^{2+} activity is also critical to the early patterns of synaptic maturation and afferent innervation during cochlear development. We also found that the increased number of ribbons did not persist in the adult mice. Since several studies have shown that a high percentage of type II afferent terminals is not associated with OHC presynaptic ribbons (Liberman et al., 1990; Martinez-Monedero et al., 2016; Vyas et al., 2017; Weisz et al., 2012), the number of type II afferent fibres in adult mice needs further investigation. Type II afferents have been suggested as cochlear nociceptors to detect tissue damage (Flores et al., 2015; Liu et al., 2015), and thus if higher numbers of type II afferents persist in adult $Ocm^{-/-}$, they could have a higher sensitivity to noise exposure.

In summary, the lack of OCM downregulates $Ca_v1.3$ channels in OHCs and upregulates P2X2 receptors in the cochlea. Without OCM expression at P2, spontaneous Ca^{2+} activity in OHCs is higher and more synchronized with the GER. We conclude that the lack of OCM changes Ca^{2+} signalling in immature OHCs, resulting in delayed synaptic pruning and changed afferent innervation during the pre-hearing period. We propose that OCM prevents Ca^{2+} overloading and regulates Ca^{2+} signalling necessary for the correct synaptic maturation and afferent innervation during development.

Figure 9. Afferent fibres increased in $Ocm^{-/-}$ at P10
A and *B*, maximum intensity projections of confocal *z*-stacks from the apical coil of the cochlea of $Ocm^{+/+}$ and $Ocm^{-/-}$ mice at P6 and P10. Afferent fibres labelled with peripherin (white) and DAPI (blue) are shown. The outer spiral fibres of type II spiral ganglion neurons travel toward the cochlear base (arrows). *C* and *D*, the mean number of tunnel crossing afferent fibres from mice of both genotypes at P6 and P10. At P6, 3 animals for each genotype, ns $P = 0.375$, *t* test; at P10, 4 animals for each genotype, ***$P = 0.002$, *t* test.

References

Babola, T. A., Li, S., Wang, Z., Kersbergen, C. J., Elgoyhen, A. B., Coate, T. M., & Bergles, D. E. (2021). Purinergic signaling controls spontaneous activity in the auditory system throughout early development. *Journal of Neuro-Science*, **41**(4), 594–612.

Balland, B., Lachamp, P., Strube, C., Kessler, J.-P., & Tell, F. (2006). Glutamatergic synapses in the rat nucleus tractus solitarii develop by direct insertion of calcium-impermeable AMPA receptors and without activation of NMDA receptors. *The Journal of Physiology*, **574**(1), 245–261.

Banville, D., & Boie, Y. (1989). Retroviral long terminal repeat is the promoter of the gene encoding the tumor-associated calcium-binding protein oncomodulin in the rat. *Journal of Molecular Biology*, **207**(3), 481–490.

Blankenship, A. G., & Feller, M. B. (2010). Mechanisms underlying spontaneous patterned activity in developing neural circuits. *Nature Reviews Neuroscience*, **11**(1), 18–29.

Bobbin, R. P. (2001). ATP-induced movement of the stalks of isolated cochlear Deiters' cells. *Neuroreport*, **12**(13), 2923–2926.

Burnstock, G. (2016). P2X ion channel receptors and inflammation. *Purinergic Signalling*, **12**(1), 59–67.

Ceriani, F., Hendry, A., Jeng, J. Y., Johnson, S. L., Stephani, F., Olt, J., Holley, M. C., Mammano, F., Engel, J., Kros, C. J., Simmons, D. D., & Marcotti, W. (2019). Coordinated calcium signalling in cochlear sensory and non-sensory cells refines afferent innervation of outer hair cells. *EMBO Journal*, **38**(9), e99839.

Chen, T.-W., Wardill, T. J., Sun, Y., Pulver, S. R., Renninger, S. L., Baohan, A., Schreiter, E. R., Kerr, R. A., Orger, M. B., Jayaraman, V., Looger, L. L., Svoboda, K., & Kim, D. S. (2013). Ultrasensitive fluorescent proteins for imaging neuronal activity. *Nature*, **499**(7458), 295–300.

Clause, A., Kim, G., Sonntag, M., Weisz, C. J., Vetter, D. E., Rubsamen, R., & Kandler, K. (2014). The precise temporal pattern of prehearing spontaneous activity is necessary for tonotopic map refinement. *Neuron*, **82**(4), 822–835.

Climer, L. K., Cox, A. M., Reynolds, T. J., & Simmons, D. D. (2019). Oncomodulin: The enigmatic parvalbumin protein. *Frontiers in Molecular Neuroscience*, **12**, 235.

Climer, L. K., Hornak, A. J., Murtha, K., Yang, Y., Cox, A. M., Simpson, P. L., Le, A., & Simmons, D. D. (2021). Deletion of oncomodulin gives rise to early progressive cochlear dysfunction in C57 and CBA Mice. *Frontiers in Aging Neuroscience*, **13**, 749729.

Cox, B. C., Liu, Z., Lagarde, M. M. M., & Zuo, J. (2012). Conditional gene expression in the mouse inner ear using Cre-loxP. *Journal of the Association for Research in Otolaryngology*, **13**(3), 295–322.

Cui, G., Meyer, A. C., Calin-Jageman, I., Neef, J., Haeseleer, F., Moser, T., & Lee, A. (2007). Ca^{2+}-binding proteins tune Ca^{2+}-feedback to Cav1.3 channels in mouse auditory hair cells. *The Journal of Physiology*, **585**(3), 791–803.

Dallos, P. (1992). The active cochlea. *Journal of Neuroscience*, **12**(12), 4575–4585.

Fechner, F. P., Nadol, J. J., Burgess, B. J., & Brown, M. C. (2001). Innervation of supporting cells in the apical turns of the guinea pig cochlea is from type II afferent fibers. *Journal of Comparative Neurology*, **429**(2), 289–298.

Flores, E. N., Duggan, A., Madathany, T., Hogan, A. K., Marquez, F. G., Kumar, G., Seal, R. P., Edwards, R. H., Liberman, M. C., & Garcia-Anoveros, J. (2015). A non-canonical pathway from cochlea to brain signals tissue-damaging noise. *Current Biology*, **25**(5), 606–612.

Glowatzki, E., Ruppersberg, J. P., Zenner, H. P., & Rusch, A. (1997). Mechanically and ATP-induced currents of mouse outer hair cells are independent and differentially blocked by d-tubocurarine. *Neuropharmacology*, **36**(9), 1269–1275.

Guinan, J. J., Jr (2018). Olivocochlear efferents: Their action, effects, measurement and uses, and the impact of the new conception of cochlear mechanical responses. *Hearing Research*, **362**, 38–47.

Hackney, C. M., Mahendrasingam, S., Penn, A., & Fettiplace, R. (2005). The concentrations of calcium buffering proteins in mammalian cochlear hair cells. *Journal of Neuroscience*, **25**(34), 7867–7875.

Hafidi, A. (1998). Peripherin-like immunoreactivity in type II spiral ganglion cell body and projections. *Brain Research*, **805**(1–2), 181–190.

Hafidi, A., & Dulon, D. (2004). Developmental expression of Cav1.3 (α1d) calcium channels in the mouse inner ear. *Developmental Brain Research*, **150**(2), 167–175.

Housley, G. D., Bringmann, A., & Reichenbach, A. (2009). Purinergic signaling in special senses. *Trends in Neuroscience (Tins)*, **32**(3), 128–141.

Housley, G. D., Luo, L., & Ryan, A. F. (1998). Localization of mRNA encoding the P2X2 receptor subunit of the adenosine 5'-triphosphate-gated ion channel in the adult and developing rat inner ear by in situ hybridization. *Journal of Comparative Neurology*, **393**(4), 403–414.

Huang, L. C., Ryan, A. F., Cockayne, D. A., & Housley, G. D. (2006). Developmentally regulated expression of the P2X3 receptor in the mouse cochlea. *Histochemistry and Cell Biology*, **125**(6), 681–692.

Jarlebark, L. E., Housley, G. D., Raybould, N. P., Vlajkovic, S., & Thorne, P. R. (2002). ATP-gated ion channels assembled from P2X2 receptor subunits in the mouse cochlea. *Neuroreport*, **13**(15), 1979–1984.

Jeng, J. Y., Ceriani, F., Hendry, A., Johnson, S. L., Yen, P., Simmons, D. D., Kros, C. J., & Marcotti, W. (2020). Hair cell maturation is differentially regulated along the tonotopic axis of the mammalian cochlea. *The Journal of Physiology*, **598**(1), 151–170.

Johny, M. B., Yang, P. S., Bazzazi, H., & Yue, D. T. (2013). Dynamic switching of calmodulin interactions underlies Ca^{2+} regulation of CaV1.3 channels. *Nature Communications*, **4**(1), 1717.

Kim, S.-H., Bahia, P. K., Patil, M., Sutton, S., Sowells, I., Hadley, S. H., Kollarik, M., & Taylor-Clark, T. E. (2020). Development of a mouse reporter strain for the purinergic P2X$_2$ receptor. *ENEURO*, **7**(4). https://doi.org/10.1523/ENEURO.0203-20.2020

Köles, L., Szepesy, J., Berekméri, E., & Zelles, T. (2019). Purinergic signaling and cochlear injury-targeting the immune system? *International Journal of Molecular Sciences*, **20**(12), 2979.

Lelli, A., Asai, Y., Forge, A., Holt, J. R., & Geleoc, G. S. (2009). Tonotopic gradient in the developmental acquisition of sensory transduction in outer hair cells of the mouse cochlea. *Journal of Neurophysiology*, **101**(6), 2961–2973.

Liberman, M. C., Dodds, L. W., & Pierce, S. (1990). Afferent and efferent innervation of the cat cochlea: Quantitative analysis with light and electron microscopy. *Journal of Comparative Neurology*, **301**(3), 443–460.

Linden, J., Koch-Nolte, F., & Dahl, G. (2019). Purine release, metabolism, and signaling in the inflammatory response. *Annual Review of Immunology*, **37**(1), 325–347.

Lippe, W. (1994). Rhythmic spontaneous activity in the developing avian auditory system. *The Journal of Neuroscience*, **14**(3), 1486–1495.

Liu, C., Glowatzki, E., & Fuchs, P. A. (2015). Unmyelinated type II afferent neurons report cochlear damage. *Proceedings of the National Academy of Sciences, USA*, **112**(47), 14723–14727.

Lukasz, D., & Kindt, K. S. (2018). In vivo calcium imaging of lateral-line hair cells in larval zebrafish. *Journal of Visualized Experiments*. (141). https://doi.org/10.3791/58794

MacManus, J. P., Whitfield, J. F., Boynton, A. L., Durkin, J. P., & Swierenga, S. H. (1982). Oncomodulin–a widely distributed, tumour-specific, calcium-binding protein. *Oncodevelopmental Biology and Medicine*, **3**(2–3), 79–90.

Maison, S. F., Liu, X. P., Eatock, R. A., Sibley, D. R., Grandy, D. K., & Liberman, M. C. (2012). Dopaminergic signaling in the cochlea: Receptor expression patterns and deletion phenotypes. *Journal of Neuroscience*, **32**(1), 344–355.

Martinez-Monedero, R., Liu, C., Weisz, C., Vyas, P., Fuchs, P. A., & Glowatzki, E. (2016). GluA2-containing AMPA receptors distinguish ribbon-associated from ribbonless afferent contacts on rat cochlear hair cells. *eNeuro*, **3**(2), ENEURO.0078-16.2016.

Melgar-Rojas, P., Alvarado, J. C., Fuentes-Santamaria, V., Gabaldon-Ull, M. C., & Juiz, J. M. (2015). Validation of reference genes for RT-qPCR analysis in noise-induced hearing loss: A study in wistar rat. *PLoS ONE*, **10**(9), e0138027.

Michanski, S., Smaluch, K., Steyer, A. M., Chakrabarti, R., Setz, C., Oestreicher, D., Fischer, C., Möbius, W., Moser, T., Vogl, C., & Wichmann, C. (2019). Mapping developmental maturation of inner hair cell ribbon synapses in the apical mouse cochlea. *Proceedings of the National Academy of Sciences, USA*, **116**(13), 6415–6424.

Michna, M., Knirsch, M., Hoda, J. C., Muenkner, S., Langer, P., Platzer, J., Striessnig, J., & Engel, J. (2003). Cav1.3 (α1D) Ca^{2+} currents in neonatal outer hair cells of mice. *The Journal of Physiology*, **553**(3), 747–758.

Mulvaney, J., & Dabdoub, A. (2012). Atoh1, an essential transcription factor in neurogenesis and intestinal and inner ear development: Function, regulation, and context dependency. *Journal of the Association for Research in Otolaryngology*, **13**(3), 281–293.

Murtha, K. E., Yang, Y., Ceriani, F., Jeng, J. Y., Climer, L. K., Jones, F., Charles, J., Devana, S. K., Hornak, A. J., Marcotti, W., & Simmons, D. D. (2022). Oncomodulin (OCM) uniquely regulates calcium signaling in neonatal cochlear outer hair cells. *Cell Calcium*, **105**, 102613.

Nikolic, P., Housley, G. D., & Thorne, P. R. (2003). Expression of the P2X7 receptor subunit of the adenosine 5'-triphosphate-gated ion channel in the developing and adult rat cochlea. *Audiology & Neuro-Otology*, **8**(1), 28–37.

Pangrsic, T., Gabrielaitis, M., Michanski, S., Schwaller, B., Wolf, F., Strenzke, N., & Moser, T. (2015). EF-hand protein Ca^{2+} buffers regulate Ca^{2+} influx and exocytosis in sensory hair cells. *Proceedings of the National Academy of Sciences, USA*, **112**(9), E1028–1037.

Platzer, J., Engel, J., Schrott-Fischer, A., Stephan, K., Bova, S., Chen, H., Zheng, H., & Striessnig, J. (2000). Congenital deafness and sinoatrial node dysfunction in mice lacking class D L-type Ca^{2+} channels. *Cell*, **102**(1), 89–97.

Roger, S., Pelegrin, P., & Surprenant, A. (2008). Facilitation of P2X7 receptor currents and membrane blebbing via constitutive and dynamic calmodulin binding. *Journal of Neuroscience*, **28**(25), 6393–6401.

Sander, S., Müller, I., Garcia-Alai, M. M., Nicke, A., & Tidow, H. (2022). New insights into P2X7 receptor regulation: Ca^{2+}-calmodulin and GDP bind to the soluble P2X7 ballast domain. *Journal of Biological Chemistry*, **298**(10), 102495.

Schmittgen, T. D., & Livak, K. J. (2008). Analyzing real-time PCR data by the comparative C(T) method. *Nature Protocols*, **3**(6), 1101–1108.

Sheets, L., Kindt, K. S., & Nicolson, T. (2012). Presynaptic CaV1.3 channels regulate synaptic ribbon size and are required for synaptic maintenance in sensory hair cells. *Journal of Neuroscience*, **32**(48), 17273–17286.

Shilling-Scrivo, K., Mittelstadt, J., & Kanold, P. O. (2021). Altered response dynamics and increased population correlation to tonal stimuli embedded in noise in aging auditory cortex. *Journal of Neuroscience*, **41**(46), 9650–9668.

Simmons, D. D. (1994). A transient afferent innervation of outer hair cells in the postnatal cochlea. *Neuroreport*, **5**(11), 1309–1312.

Simmons, D. D., Mansdorf, N. B., & Kim, J. H. (1996). Olivocochlear innervation of inner and outer hair cells during postnatal maturation: Evidence for a waiting period. *Journal of Comparative Neurology*, **370**(4), 551–562.

Simmons, D. D., Tong, B., Schrader, A. D., & Hornak, A. J. (2010). Oncomodulin identifies different hair cell types in the mammalian inner ear. *Journal of Comparative Neurology*, **518**(18), 3785–3802.

Spitzer, N. C. (2006). Electrical activity in early neuronal development. *Nature*, **444**(7120), 707–712.

Tong, B., Hornak, A. J., Maison, S. F., Ohlemiller, K. K., Liberman, M. C., & Simmons, D. D. (2016). Oncomodulin, an EF-Hand Ca^{2+} Buffer, is critical for maintaining cochlear function in mice. *Journal of Neuroscience*, **36**(5), 1631–1635.

Tritsch, N. X., Yi, E., Gale, J. E., Glowatzki, E., & Bergles, D. E. (2007). The origin of spontaneous activity in the developing auditory system. *Nature*, **450**(7166), 50–55.

Vlajkovic, S. M., & Thorne, P. R. (2022). Purinergic signalling in the cochlea. *International Journal of Molecular Sciences*, **23**(23), 14874.

Vyas, P., Wu, J. S., Zimmerman, A., Fuchs, P., & Glowatzki, E. (2017). Tyrosine hydroxylase expression in type II cochlear afferents in mice. *Journal of the Association for Research in Otolaryngology*, **18**(1), 139–151.

Wang, J. C., Raybould, N. P., Luo, L., Ryan, A. F., Cannell, M. B., Thorne, P. R., & Housley, G. D. (2003). Noise induces up-regulation of P2X2 receptor subunit of ATP-gated ion channels in the rat cochlea. *Neuroreport*, **14**(6), 817–823.

Weisz, C. J., Lehar, M., Hiel, H., Glowatzki, E., & Fuchs, P. A. (2012). Synaptic transfer from outer hair cells to type II afferent fibers in the rat cochlea. *Journal of Neuroscience*, **32**(28), 9528–9536.

Yang, H., Xie, X., Deng, M., Chen, X., & Gan, L. (2010). Generation and characterization of Atoh1-Cre knock-in mouse line. *Genesis*, **48**(6), 407–413.

Zuccotti, A., Lee, S. C., Campanelli, D., Singer, W., Satheesh, S. V., Patriarchi, T., Geisler, H.-S., Köpschall, I., Rohbock, K., Nothwang, H. G., Hu, J., Hell, J. W., Schimmang, T., Rüttiger, L., & Knipper, M. (2013). L-type CaV1.2 deletion in the cochlea but not in the brainstem reduces noise vulnerability: Implication for CaV1.2-mediated control of cochlear BDNF expression. *Frontiers in Molecular Neuroscience*, **6**, 20.

Zuo, H., Cui, B., She, X., & Wu, M. (2008). Changes in Guinea pig cochlear hair cells after sound conditioning and noise exposure. *Journal of Occupational Health*, **50**(5), 373–379.

Additional information

Data availability statement

The data that support the findings of this study are available from the corresponding author upon reasonable request.

Competing interests

The authors declare no conflicts of interest.

Author contributions

Y.Y.: formal analysis; investigation; methodology; software; visualization; writing – original draft; writing – review and editing. K.E.M.: investigation; methodology; writing – review and editing. L.K.C: methodology; validation; writing – review and editing. F.C.: methodology; validation; formal analysis; writing – review and editing. P.T.: investigation; methodology; writing – review and editing. A.J.H.: project administration; investigation; writing–review and editing. W.M.: conceptualization; methodology; software; resources; writing–review and editing; supervision; project administration; funding acquisition. D.D.S.: conceptualization; methodology;

Supporting information

Additional supporting information can be found online in the Supporting Information section at the end of the HTML view of the article. Supporting information files available:

Statistical Summary Document
Peer Review History
Movie 1
Movie 2
Movie 3